pp 1231–1244. © The Author(s), 2021. Published by Cambridge University Press on behalf of Royal Aeronautical Society.
doi:10.1017/aer.2021.9

Moving-mass-based station keeping of stratospheric airships

L. Chen
cl200432@tom.com
School of Air Transportation,
Shanghai University of Engineering Science,
Shanghai,
China
and
State Key Laboratory of Robotics,
Shenyang Institute of Automation,
Chinese Academy of Sciences,
Shenyang,
China

Q. Gao and Y. Deng
School of Air Transportation,
Shanghai University of Engineering Science,
Shanghai,
China

J. Liu
State Key Laboratory of Robotics,
Shenyang Institute of Automation,
Chinese Academy of Sciences,
Shenyang,
China

ABSTRACT

Stratospheric airships are lighter-than-air vehicles that work at an altitude of 20km in the lower calm portion of the stratosphere. They can be used as real-time surveillance platforms for environment monitoring and civil communication. Solar energy is the ideal power choice for long-endurance stratospheric airships. Attitude control is important for airships so that they can point at a target for observation or adjust the attitude to improve the output performance of solar panels. Stratospheric airships have a large volume and semi-flexible structure. The typical actuators used are aerodynamic surfaces, vectored thrust and ballonets. However, not

Received 11 September 2019; revised 19 December 2020; accepted 1 February 2021.

all these actuators can work well under special working conditions, such as low density and low speed. In this study, moving-mass control is introduced to stratospheric airships because its control efficiency is independent of airspeed and atmospheric density. A nonlinear feedback controller based on generalised inverse with a nonlinear mapping module is designed to implement moving-mass control. Such a new station keeping scheme with moving masses is proposed for airships with different working situations.

Keywords: Stratospheric airship platform; Moving-mass control; Station keeping; Attitude control

NOMENCLATURE

m_{lon},	mass of the longitudinal moving mass
m_{lat},	mass of the lateral moving mass
m_B,	mass of the airship body B except the moving mass
m_S,	mass of the whole system S
μ_{lon},	mass ratio of longitudinal moving mass to the whole system
μ_{lat},	mass ratio of lateral moving mass to the whole system
μ_B,	mass ratio of airship body to the whole system
$\mathbf{P_B}$,	position vector of the mass centre of B in the body frame
$\mathbf{P_S}$,	position vector of the mass centre of S in the body frame
$\mathbf{P_{lon}}$,	position vector of the longitudinal moving mass in the body frame
$\mathbf{P_{lat}}$,	position vector of the lateral moving mass in the body frame
$\mathbf{X}$,	vector of state variations
$\mathbf{U}$,	indirect control vector
$\mathbf{Y}$,	output vector
$\mathbf{M}$,	mass matrix
$\mathbf{M_T}$,	transform matrix
m_{ij},	added masses of the airship
T_Z,	control forces along the z-axis
T_D,	control differential thrust about the z-axis
T_{cl},	left vectored thrust
T_{cr},	right vectored thrust
δ_{cr},	right vectored angle
δ_{cl},	left vectored angle
Δ_{cof},	mass coefficient matrix
x_{lon},	x-position of longitudinal moving mass
y_{lat},	y-position of lateral moving mass
h,	flight altitude of the airship
$x, y, z, \phi, \theta, \psi$,	inertial position and Euler angle
u, v, w, p, q, r,	linear and angular velocities in the body-fixed frame
Vx, Vy, Vz,	linear velocity in the inertia-fixed frame

https://doi.org/10.1017/aer.2021.9 Published online by Cambridge University Press

1.0 INTRODUCTION

Stratospheric airships can be used as real-time surveillance platforms for environment monitoring and civil communication at a working altitude of 20km[1,2]. Solar energy is the ideal power choice for long-endurance stratospheric airships. The output performance of solar array on stratospheric airships is affected by airship's attitude. A key technical challenge for stratospheric platforms is autonomous station keeping or the ability to remain fixed over a geolocation in the presence of winds. Attitude control systems, which are a necessary part of airship systems, mainly implement two functions. One function is to enable pointing at the ground target for observation; another function is to adjust the attitude to improve the output performance of solar panels[3,4].

The typical actuators used are aerodynamic control surfaces, vectored thrust and ballonets[5,6]; however, not all these actuators can work well under special working conditions, such as low density and low speed. Most studies in this field emphasise composite control with multiple actuators. Liu[7] investigated the feasibility and stability of equilibrium flight of an airship in a longitudinal plane equipped with ballonets and ballast. Fan[8] studied the altitude control system of a high-altitude airship with an auxiliary ballonet and an elevator. Guo[9] presented a design method for stratospheric airships with an aircrew propeller and aerodynamic surface. Di[10] established a method to solve the problem of attitude control given an aerodynamic fin and vectored thruster. Chen[11] provided the attitude moment allocation between aerodynamic surfaces and vectored propellers by using weighted generalised inverse (GI) methods. The above-mentioned studies focused on pitch control but did not consider roll control because of the limited control authority of existing actuators.

Moving-mass control is a method that can change external moment by displacing the internal masses of the aircraft to change its centre of mass. Through this method, the attitude of aircraft can be changed. Successful applications can be found in studies on spacecraft[12], reentry vehicles[13], underwater vehicles[14], Kinetic Kill Vehicles (KKV)[15], saucer-like air vehicles[16] and missiles[17]. This idea is also reflected in low-altitude airship control[18]. In the field of stratospheric airships, application involving moving mass control was first reported publicly in our research, which referred to Chen[19], in which the moving-mass control scheme and dynamics for stratospheric airships were presented and a nonlinear composite controller with aerodynamic control surfaces, moving mass and vectored thrust for pitch control was considered. Subsequently, ascending and descending schemes for a stratospheric airship based on pitch control were proposed, where the pitch angle is controlled by ballonets and elevators[20].

This study is a continuation of our previous work[19]. To achieve attitude control for station keeping in still air, two moving masses are used for roll and pitch regulation, whereas the altitude and yaw angle are regulated by two vectored thrusters. The paper is structured as follows: section 1 introduces the composite control state of stratospheric airships. Section 2 details the configuration of an airship with moving masses and presents the whole system's mass centre with the positions of the moving masses. The design process of an attitude controller in station keeping is considered in section 3. The performance of station keeping is then tested by simulation in section 4. Lastly, section 5 concludes the study with some observations.

https://doi.org/10.1017/aer.2021.9 Published online by Cambridge University Press

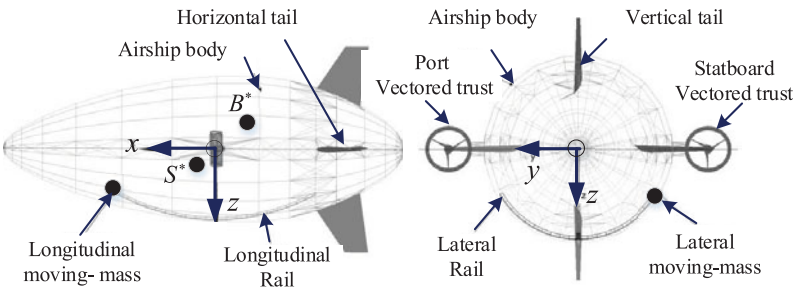

Figure 1. Stratospheric airship with moving masses.

2.0 MOVING-MASS SCHEME

For a stratospheric airship with a length of 170m, a moving-mass scheme of two moving masses is designed. The moving-mass actuator comprises two rails installed along the envelope bottom, with two moving masses moving freely on the rails. The configuration of the airship and moving-mass module is shown in Fig. 1[19].

The mass of the airship body B is m_B, and the masses of the longitudinal and lateral moving masses are m_{lon} and m_{lat}, respectively. The mass of the system S is m_S, where $m_S = m_B + m_{lon} + m_{lat}$. The mass ratios are defined as $\mu_B = \frac{m_B}{m_S}$, $\mu_{lon} = \frac{m_{lon}}{m_S}$ and $\mu_{lat} = \frac{m_{lat}}{m_S}$. As shown in Fig. 1, the mass centre of B is B^*, which is fixed and independent of the motion of the moving masses; the mass centre of S is S^*, which is displaced with motion of the moving masses. The position vectors of B^* and S^* in the body frame are $\mathbf{P_B} = (x_G, y_G, z_G)$ and $\mathbf{P_S} = (x'_G, y'_G, z'_G)$, respectively. The two rails are located in the xOz and yOz planes of the body frame, such that the position vectors of the longitudinal and lateral moving masses can be set at $\mathbf{P_{lon}} = (x_{lon}, 0, z_{lon})$ and $\mathbf{P_{lat}} = (0, y_{lat}, z_{lat})$, respectively. The relationship of $\mathbf{P_S}$ with $\mathbf{P_B}$, $\mathbf{P_{lon}}$ and $\mathbf{P_{lat}}$ is $\mathbf{P_S} = \frac{m_B\mathbf{P_B} + m_{lon}\mathbf{P_{lon}} + m_{lat}\mathbf{P_{lat}}}{m_S}$, where $\mathbf{P_B}$ is fixed for a given airship body, and $\mathbf{P_S}$ varies with the position of moving masses $\mathbf{P_{lon}}$ and $\mathbf{P_{lat}}$.

3.0 ATTITUDE CONTROLLER FOR STATION KEEPING

The current study investigates the attitude control of airships during station keeping. With respect to energy and mass constraints, stratospheric airships have a low thrust-to-weight ratio. When they take off from the ground, their ultimate altitude is determined by the net lift/weight, whereas the horizontal position is uncontrolled. While flying at a working altitude of 20km, as a real-time surveillance platform, they should have the ability to change attitude to meet the mission requirements. Meanwhile, if the altitude is maintained, then high-resolution observations can be achieved. Here, pitch and roll are controlled by the moving masses, whereas yaw and altitude are regulated by two vectored thrusters. Since airship operation in still air is assumed, horizontal position control is not considered; however, it is indirectly influenced by attitude control. Aerodynamic surfaces are not effective at low airspeeds for station keeping.

3.1 Attitude controller structure

This section proposes the design procedure of a nonlinear control system for airships. The nonlinear composite control system is depicted in Fig. 2; it consists of two basic structures: one for altitude holding and another for attitude regulation. The input of altitude holding is the

https://doi.org/10.1017/aer.2021.9 Published online by Cambridge University Press

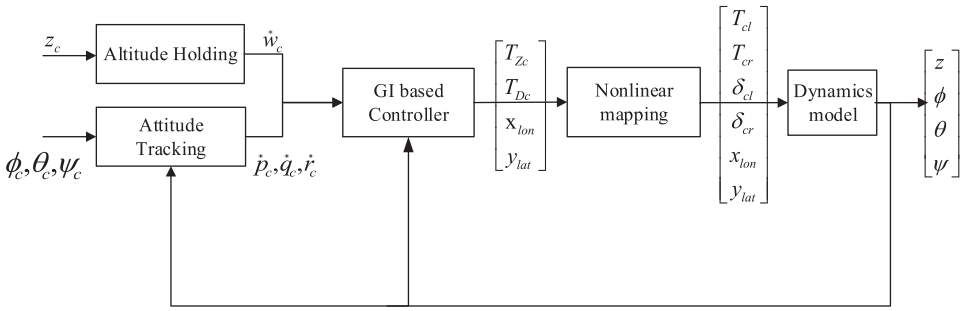

Figure 2. Nonlinear controller structure.

expected altitude z_c and attitude angles $\phi_c \theta_c \psi_c$; the output is the desired linear acceleration $\dot{w}_c$ and angular accelerations $\dot{p}_c$, $\dot{q}_c$ and $\dot{r}_c$, which are responsible for tracking the expected altitude and attitude. The controller is designed on the basis of output feedback linearisation control; the output of the system is $\mathbf{Y} = \left[z\ \phi\ \theta\ \psi\right]^{\mathrm{T}}$. The output of the controller is the altitude regulation forces along the z-axis T_{Zc} and differential thrust around the z-axis T_{Dc} and the positions of the longitudinal and lateral moving masses x_{lon}, y_{lat}. The nonlinear mapping module transforms the control forces along the z-axis T_{Zc} and differential thrust around the z-axis T_{Dc} to the independent outputs of every thrust $\left[\ T_{cl}\ T_{cr}\ \delta_{cl}\ \delta_{cr}\ \right]^{\mathrm{T}}$.

3.2 GI-based attitude controller

Generally, airship dynamics can be expressed as

$$\begin{aligned} \dot{\mathbf{X}} &= \mathbf{f(X)} + \mathbf{g(X)U} \\ \dot{\mathbf{Y}} &= \mathbf{h(X)} \end{aligned} \quad \ldots (1)$$

where $\mathbf{X} = (w, p, q, r)^{\mathrm{T}}$ is a four-dimension state vector, $\mathbf{U} = [T_Z, T_D, x_{lon}, y_{lat}]^{\mathrm{T}}$ is a direct control vector and $\mathbf{Y} = [z, \phi, \theta, \psi]^{\mathrm{T}}$ is an output vector. $\mathbf{f} = \mathbf{f(X)}$ is a nonlinear state-dependent function; $\mathbf{g} = \mathbf{g(X)}$ is independent of the control variable, as shown in Equation (2); details of the dynamic model can be seen in Chen[19].

$$\mathbf{g(X)} = \begin{bmatrix} g_0(X) \\ g_1(X) \\ g_2(X) \\ g_3(X) \end{bmatrix} = \mathbf{\Delta_{cof}^{-1}} \cdot \begin{bmatrix} 1 & 0 & 0 & 0 \\ 0 & 0 & 0 & \mu_{lat}\mathrm{G}\cos\phi\cos\theta \\ x_{Tcr} & 0 & \mu_{lat}\mathrm{G}\cos\phi\cos\theta & 0 \\ 0 & y_{\mathrm{s}} & \mu_{lat}\mathrm{G}\cos\phi\cos\theta & \mu_{lat}\mathrm{G}\sin\theta \end{bmatrix} \quad \ldots (2)$$

where $\Delta_{\mathbf{cof}} = diag(m_s + m_{33}, I_x + m_{44}, I_y + m_{55}, I_z + m_{66})$ is the mass coefficient matrix, and (x_s, y_s, z_s) is the position of the side vectored thrust in the body frame; here, $x_s{=}z_s{=}0$. The derivation of $\mathbf{Y}$ is defined by $\ddot{\mathbf{Y}} = \mathbf{h_X}\dot{\mathbf{X}} = \mathbf{h_X}(\mathbf{f} + \mathbf{gU})$, where $\mathbf{h_X} = \frac{\partial \mathbf{h(X)}}{\partial \mathbf{X}}$. For a given commanded input $\mathbf{Y_c}{=}[z_c, \phi_c, \theta_c, \psi_c]^{\mathrm{T}}$, the desired behaviour of a closed system is defined by $\mathbf{Y}_{\mathrm{d}} = ff(\mathbf{Y}, \mathbf{Y_c})$. Here, $ff()$ is designed as a Proportional–Integral–Differential (PID) controller to obtain the desired accelerations of closed system $\mathbf{Y}_{\mathrm{d}} = (\ddot{z}_d, \ddot{\phi}_d, \ddot{\theta}_d, \ddot{\psi}_d)^{\mathrm{T}}$.

$$\ddot{z}_{\mathrm{d}} = k_{pz}(z_c - z) + k_{iz}\int (z_c - z)dt \quad \ldots (3)$$

https://doi.org/10.1017/aer.2021.9 Published online by Cambridge University Press

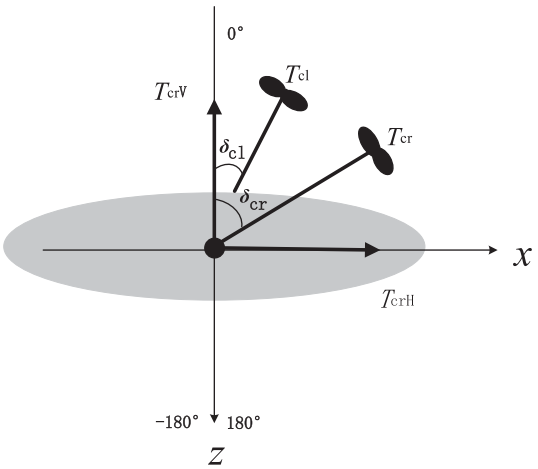

Figure 3. Vectored-thrust frame and deflection angle.

$$\ddot{\phi}_d = k_{p\phi}(\phi_c - \phi) + k_{d\phi}(\dot{\phi}_c - \dot{\phi}) + k_{i\phi}\left(\int (\phi_c - \phi)dt\right) \quad \ldots(4)$$

$$\ddot{\theta}_d = k_{p\theta}(\theta_c - \theta) + k_{d\theta}(\dot{\theta}_c - \dot{\theta}) + k_{i\theta}\left(\int (\theta_c - \theta)dt\right) \quad \ldots(5)$$

$$\ddot{\psi}_{\mathrm{d}} = k_{p\psi}(\psi_c - \psi) + k_{d\psi}(\dot{\psi}_c - \dot{\psi}) \quad \ldots(6)$$

where $k_{p\phi}$, $k_{d\phi}$, $k_{i\phi}$, $k_{p\theta}$, $k_{d\theta}$, $k_{i\theta}$, $k_{d\psi}$, $k_{p\psi}$, k_{iz} and k_{pz} are controller parameters.

By changing $\ddot{\mathbf{Y}}$ in the previous equation to track $\mathbf{Y}_{\mathrm{d}}$, the final form of a nonlinear feedback control law is obtained on the basis of the GI calculation as

$$\mathbf{U} = (\mathbf{h_X g})^{-1} \bullet (\mathbf{Y_d} - \mathbf{h_X f}) \quad \ldots(7)$$

where $(\mathbf{h_X g})^{-1}$ denotes the GI of matrix $\mathbf{h_X g}$, and $\mathbf{h_X g}$ is called the control efficiency matrix.

Given the desired altitude and attitude $\mathbf{Y_c}=[z_c, \phi_c, \theta_c, \psi_c]^{\mathrm{T}}$, the desired attitude and velocity can be deduced from the kinematics $w_c = \dot{z}_c + u\theta$, where $\dot{z}_c = k(z_c - z)$is the tracking vertical velocity; $\theta_c = c_1$, $\phi_c = c_2$, where c_1 and c_2 are the given attitude from the task requirements; and $\psi_c = \arctan(-V_{wy}/-V_{wx})$, and V_{wy}, V_{wx} are the wind components in the inertial frame along the x and y directions, respectively.

3.3 Nonlinear mapping module

The airship has two vectored thrusters with four control variables for altitude and yaw control. Thus, control allocation is necessary for two-channel synchronised control. The local vectored-thrust frame is established in the vectored-rotation plane (Fig. 3), where δ_{cl}, δ_{cr} are the deflect angle of the left and right vectored propellers, respectively; it can deflect around the installed axis at a range of $[-180°, 180°]$. T_{cl}, T_{cr} is the generated force whose amplitude is decided by the rotational speed of the propeller.

In the vectored-rotation plane, the vectored thrust can be decomposed into two orthogonal forces: $T_{\mathrm{clH}} = T_{\mathrm{cl}}\sin(\delta_{\mathrm{cl}})$, $T_{\mathrm{clV}} = -T_{\mathrm{cl}}\cos(\delta_{\mathrm{cl}})$, $T_{\mathrm{crH}} = T_{\mathrm{cr}}\sin(\delta_{\mathrm{cr}})$ and $T_{\mathrm{crV}} = -T_{\mathrm{cr}}\cos(\delta_{\mathrm{cr}})$.

https://doi.org/10.1017/aer.2021.9 Published online by Cambridge University Press

Here, T_{clH}, T_{clV}, T_{crH} and T_{crV} are called indirect control variables, and they can also be decomposed into the body-fixed frame with transform matrix

$$\mathbf{M_T} = \begin{bmatrix} 1 & 0 & 1 & 0 \\ 0 & 1 & 0 & 1 \\ 0 & y_{\mathrm{s}} & 0 & -y_{\mathrm{s}} \\ y_{\mathrm{s}} & 0 & -y_{\mathrm{s}} & 0 \end{bmatrix}.$$

Thus, we have

$$\begin{bmatrix} T_{\mathrm{X}} \\ T_Z \\ T_\phi \\ T_\psi \end{bmatrix} = \mathbf{M_T} \begin{bmatrix} T_{\mathrm{clH}} \\ T_{\mathrm{clV}} \\ T_{\mathrm{crH}} \\ T_{\mathrm{crV}} \end{bmatrix} \quad \ldots (8)$$

where T_{X}, T_Z, T_ϕ and T_ψ are the forces and moments generated by the thrusters. Here, only the altitude and yaw are controlled by the two thrusters; thus, T_Z and T_ψ are the control forces, and T_{X} and T_ϕ are considered the disturbance forces. When the controller calculates the commanded control force T_{Zc} and $T_{\psi \mathrm{c}}$, the indirect control variables can be deduced by the inverse transform of $\mathbf{M_T}$:

$$\begin{bmatrix} T_{\mathrm{clH}} \\ T_{\mathrm{clV}} \\ T_{\mathrm{crH}} \\ T_{\mathrm{crV}} \end{bmatrix} = \mathbf{M}_{\mathrm{T}}^{-1} \begin{bmatrix} 0 \\ T_{\mathrm{Zc}} \\ 0 \\ T_{\psi \mathrm{c}} \end{bmatrix} \quad \ldots (9)$$

Then, the direct control variables $T_{\mathrm{cr}} = \sqrt{T_{\mathrm{crH}}^2 + T_{\mathrm{crV}}^2}$, $T_{\mathrm{cl}} = \sqrt{T_{\mathrm{clH}}^2 + T_{\mathrm{clV}}^2}$ and $\delta_{\mathrm{cr}} = (\tan \frac{T_{\mathrm{crH}}}{T_{\mathrm{crV}}})^{-1}$, $\delta_{\mathrm{cl}} = \tan \frac{T_{\mathrm{clH}}}{T_{\mathrm{clV}}}^{-1}$ are obtained.

4.0 SIMULATION RESULTS FOR STATION KEEPING

Given that the body of an airship is similar to a spindle, that is, with a large length and round cross section, the rail in the xOz plane can be regarded as a straight line parallel to the body axis, and the rail in the yOz plane can be considered an arc. The maximum radius of the cross section is given as 25m. Hence, the position vectors of the longitudinal and lateral moving masses can be set as $P_{lon} = (x_{lon}, 0, 25)$ and $P_{lat} = (0, y_{lat}, 25\cos(\arcsin \frac{y_{lat}}{25}))$, respectively, with rail lengths $|x_{lon}| \leq 40$ and $|y_{lat}| \leq 15$. When the masses are at their initial position, $x_{lon} = y_{lat} = 0$, the moving-mass ratio is given by $\mu_{\mathrm{lon}} = 0.2$, $\mu_{\mathrm{lat}} = 0.1$.

4.1 Open-loop control

Open-loop control is given to validate the control ability of moving masses. When the airship is cruising with an initial speed of 3m/s, the masses first move to the maximum positive displacement from the initial position, then move to the maximum negative displacement, then move back to the initial position. In this process, the masses move at a constant speed, either in the positive or negative direction. The attitude and position of the airship and relative moment are observed, as shown in Figs 4 and 5.

https://doi.org/10.1017/aer.2021.9 Published online by Cambridge University Press

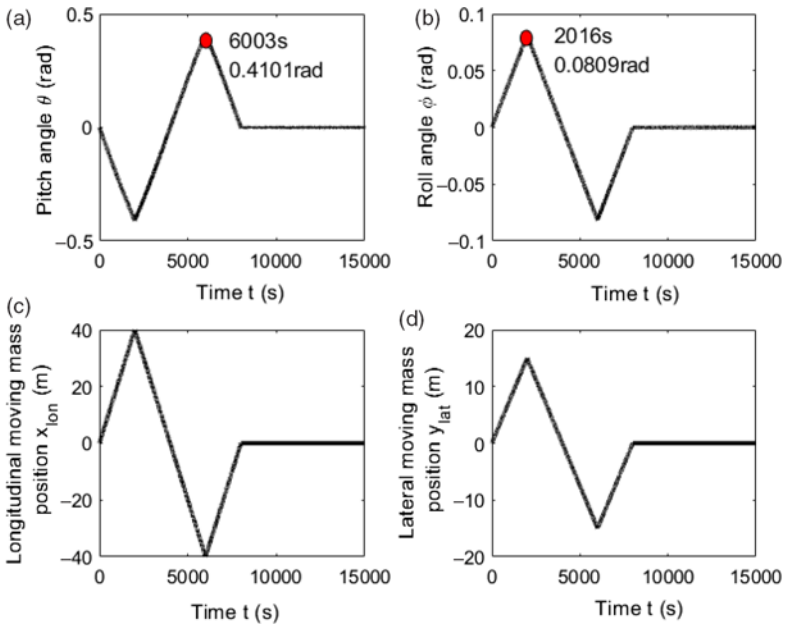

Figure 4. Attitude and position of both moving masses with open-loop control.

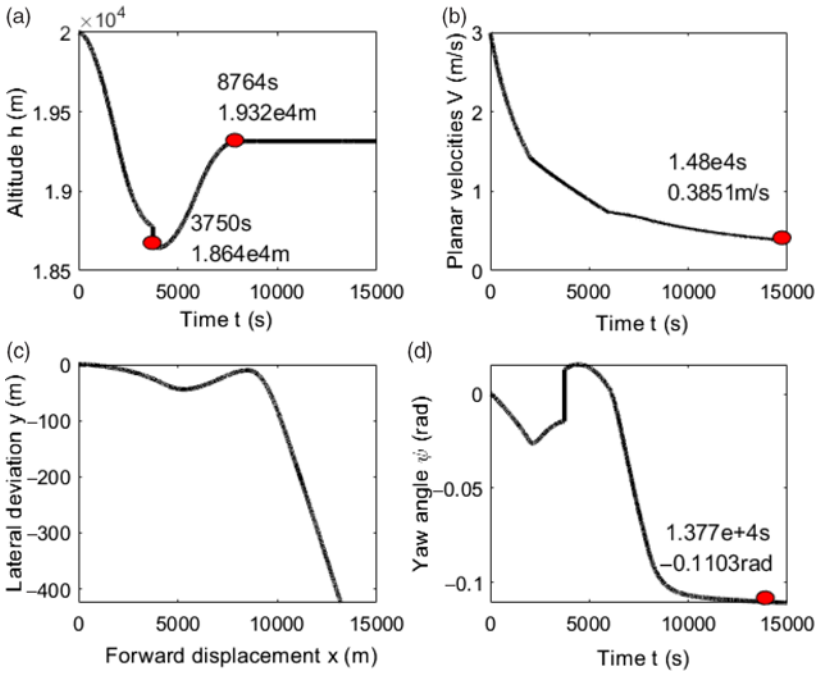

Figure 5. Position, velocity and yaw angle with open-loop control.

https://doi.org/10.1017/aer.2021.9 Published online by Cambridge University Press

Simulation results reveal that when the longitudinal moving mass is at a positive displacement in the body frame, the airship is placed in a nose-down position; when the longitudinal moving mass is at a negative displacement, the airship is placed in a nose-up position. The maximum pitch angle obtained is 0.41rad. The pitch angle induces the maximum altitude variation of 1350m downward; the plenary inertial velocity is reduced along with the pitch control, whether the airship is nose up or nose down. Similarly, the maximum roll response to movement of the lateral moving mass is 0.08rad. The airship demonstrates light damping in yaw at a low velocity. The sideslip angle induced by roll generates aerodynamic moment in the yaw direction, resulting in a change in the yaw angle; given such coupling dynamics, the roll angle induces the yaw drift of 0.109rad; thus, the airship has lateral position deviation along with roll control. As the horizontal velocity is uncontrolled, the airship's horizontal position changes with the yaw deviation and reduces its forward velocity.

The primary functional moments in this process are the gravitational and aerodynamic moments: the change in gravitational moment is attributed to the movement of the centre of mass S, whereas the change in aerodynamic moment is induced by a variation in the angle of attack and sideslip angle; detailed analyses can be seen in Chen[19].

4.2 Closed-loop control

As a real-time surveillance platform, station keeping allows the airship to stay within a certain horizontal range, whereas the altitude is maintained to achieve high-resolution observations; the pitch and roll are controlled to meet the mission requirements with respect to ground targets or to regulate the solar output, and the yaw control lets the airship head against the wind to reduce position drift or to change its course.

The given hovering altitude is $h_c = 2 \times 10^4 m$. Motion planning is considered to realise smooth manipulation, so a maximum desired height difference $\Delta h = 50m$ is selected. When $h_c - h > \Delta h$, the tracking target is the command vertical velocity $\dot{h} \to \dot{h}_c$. When $h_c - h \leq \Delta h$, the tracking target is the final position $h \to h_c$. The commanded attitude is given as follows:

$$\begin{cases} \phi_c = 0.08, \theta_c = 0.3, \psi_c = 0.2 & 0 < t \leq 2000 \\ \phi_c = 0.0, \theta_c = 0.0, \psi_c = 0.0 & 2000 < t \leq 4000 \\ \phi_c = -0.08, \theta_c = -0.3, \psi_c = -0.2 & 4000 < t \leq 6000 \\ \phi_c = 0.0, \theta_c = 0.0, \psi_c = 0.0 & 6000 < t \leq 15000 \end{cases} \quad \ldots (10)$$

The simulation results of the closed-loop attitude system are shown in Figs 6–8.

The simulation results reveal that the attitude tracks the command value on the same level that can be realised by open control, and the altitude error is controlled within 100m (Fig. 6(a)). As the yaw is controlled, the lateral deviation is controlled; the stable deviation is 253.7m for consistency with plot as shown in Fig. 7(b). As the horizontal velocity is uncontrolled, the forward velocity decreases gradually (Fig. 7(d)). Figure 7(c) shows the airflow angle, which varies with the attitude variation, such that the aerodynamic moments change.

The indirect control force and real output of every thruster are shown in Fig. 8. Two thrusters are composited to generate vertical and differential forces.

4.3 Station-keeping performance

The performance of moving-mass control in station keeping is tested under different velocities. The range of airspeed is from 0m/s to 3m/s, and the controller parameters are kept

https://doi.org/10.1017/aer.2021.9 Published online by Cambridge University Press

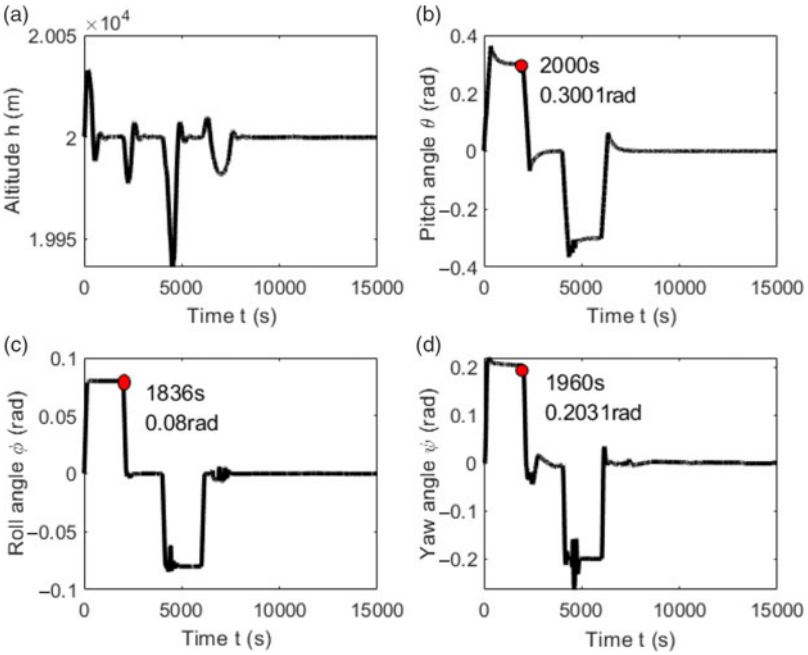

Figure 6. Altitude and attitude control with closed-loop control.

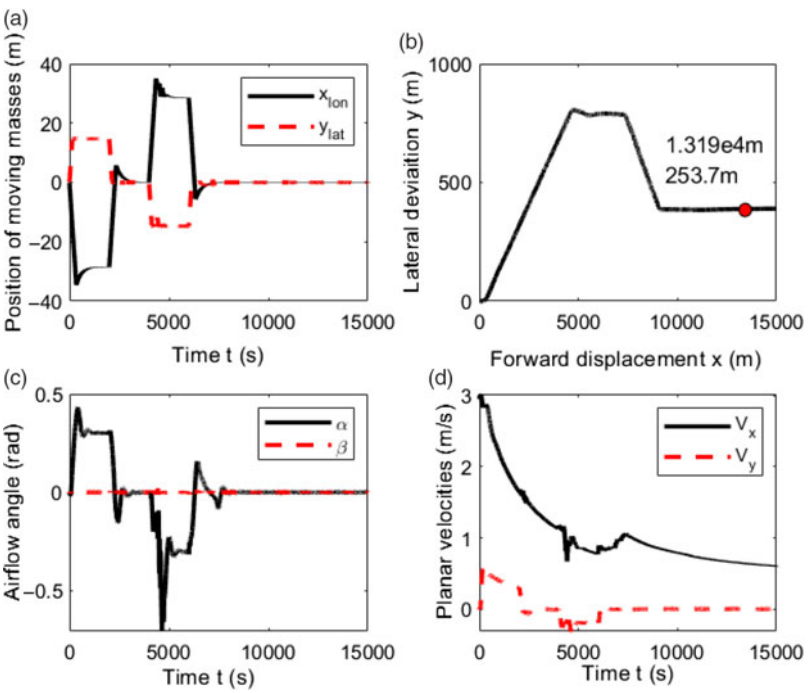

Figure 7. Position of both moving masses, lateral position, airflow angles and planar velocities with closed-loop control.

https://doi.org/10.1017/aer.2021.9 Published online by Cambridge University Press

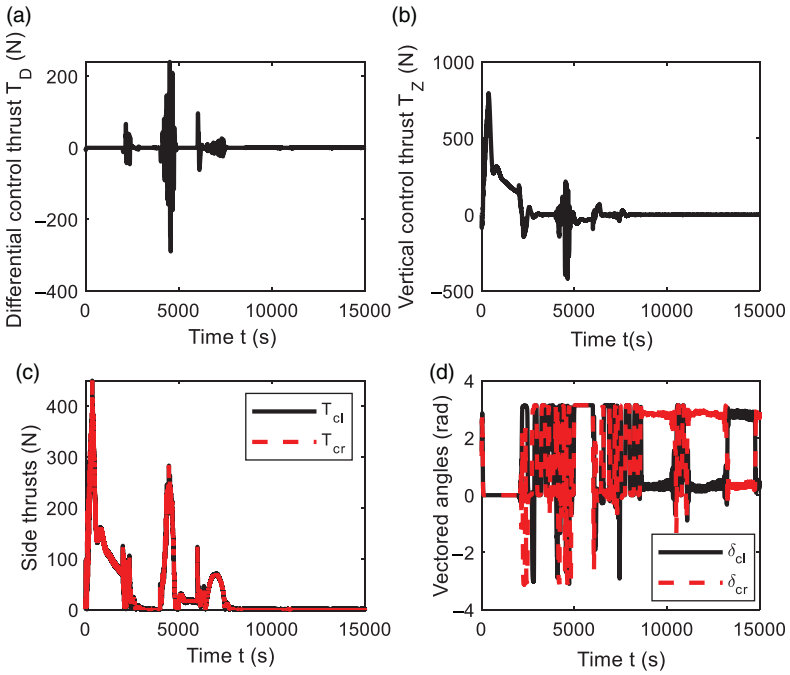

Figure 8. Output of vectored thrusters with closed-loop control.

constant in closed control. The open and closed moving-mass control results are shown in Figs 9 and 10, respectively.

As shown in Fig. 9, with an initial velocity of 0m/s (i.e. no wind), the yaw has considerable deviation (Fig. 9(d)) due to strong roll and yaw coupling; thus, the airship turns around within a small range, and the airship demonstrates light damping in yaw at a low velocity (Fig. 9(d)). With the increase in airspeed, the coupling between the pitch and the altitude is evident, the altitude changes rapidly (Fig. 9(a)) and the position range is enlarged (Fig. 9(c)).

The station-keeping performance of the closed-loop system is shown in Fig. 10; compared with the performance of open control (Fig. 9), the station-keeping range is enlarged. Nevertheless, the airship moves regularly (Fig. 10(c)), and the altitude does not fluctuate remarkably. Under normal situations, with an increase in airspeed from 0.5m/s to 3m/s, the station-keeping range is increased. Lateral deviation stops when the yaw angle is controlled to trim point. With the increase in airspeed, the closed-loop yaw control should be implemented to suppress the deviation of lateral and altitude displacements; thus, the forward displacement is enlarged, which can be seen from comparison of Fig. 9(c) and (d) with Fig. 10(c) and (d).

With an initial velocity of 0m/s, the closed-loop control system adapts to the no-wind situation; however, it does not achieve the best station-keeping performance because of the strong coupling between yaw and roll (Fig. 9(d)). In closed control, the yaw angle is controlled, such that the airship no longer turns around. Thus, the station-keeping range is enlarged, as shown in Fig. 10(c).

On the basis of the above discussion, the following conclusions can be drawn: in attitude control during station keeping, the yaw control can be chosen on the basis of the task requirements. With low airspeed (approximately 0m/s), the airship can hover within a small range

https://doi.org/10.1017/aer.2021.9 Published online by Cambridge University Press

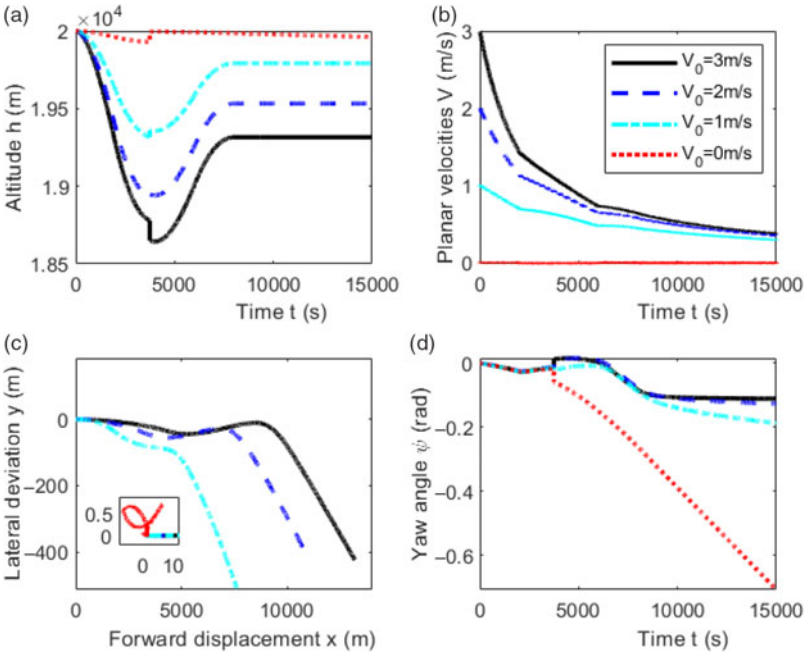

Figure 9. Station-keeping performance of the open-loop system under different velocities.

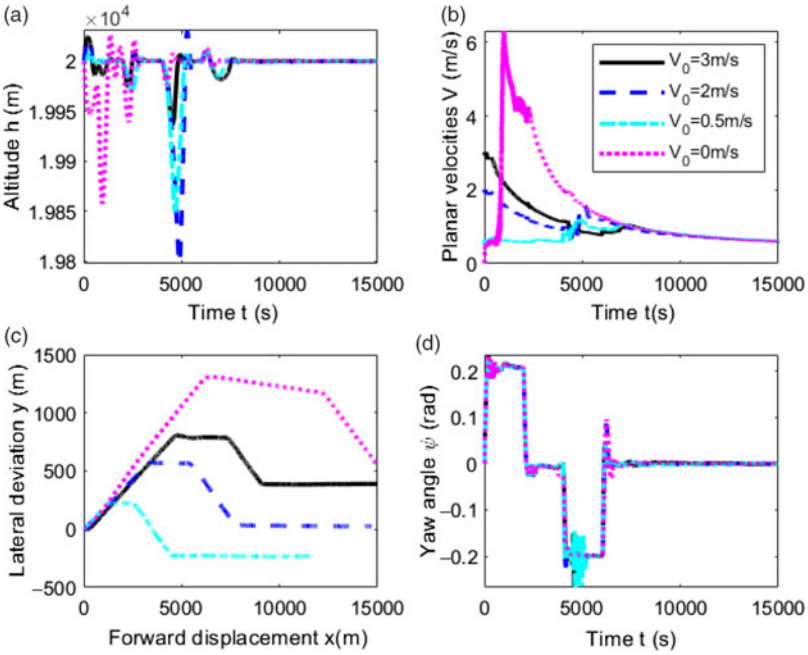

Figure 10. Station-keeping performance of the closed-loop system under different velocities.

https://doi.org/10.1017/aer.2021.9 Published online by Cambridge University Press

without yaw control. With an increase in airspeed, the yaw can be controlled to obtain stable lateral deviation, and the airship slowly moves forward with a stable altitude.

5.0 CONCLUSION

Moving-mass control is introduced to stratospheric airships for attitude control with station keeping at a given altitude. The altitude and yaw angle are regulated by two vectored thrusters, whereas the roll and pitch are controlled by two moving masses. The performance of moving-mass control in station keeping is tested under different velocities. In open-loop attitude control, the coupling between pitch and altitude and between roll and yaw is evident; thus, altitude and lateral displacements are induced. Under low airspeed, the airship can adjust its pitch and roll, hovering within a fixed range with uncontrolled yaw deviation. With an increase in airspeed, the closed-loop yaw control should be implemented to suppress the deviation of lateral and altitude displacements; thus, the forward displacement is enlarged. Nevertheless, stable station-keeping performance is guaranteed, because there is not big drift of planary positions under the assumption of still air. On the other hand, the main limitation of this controller is that the airship in still air is assumed; otherwise, the horizontal position of the airship drifts in an uncontrolled manner. If there is wind, the horizontal position of the airship needs to be controlled for station keeping. The velocity control can be implemented by extra thrusters, or a new control scheme should be proposed.

ACKNOWLEDGEMENTS

This work is supported by the National Science Foundation of China (no. 61733017) and the Foundation of State Key Laboratory of Robotics of China (no. 2018O13) and is sponsored by the Shanghai Pujiang Program (no. 18PJD018).

REFERENCES

1. SCHMIDT, D.K. Modeling and near-space station-keeping control of a large high-altitude airship. *J Guid Contr Dynam*, 2007, **30**, (2), pp 540–547.
2. YANG, X.W., YANG, X.X. and DENG, X.L. Horizontal trajectory control of stratospheric airships in wind field using Q-learning algorithm. *Aerosp Sci Technol*, 2020, **106**, pp 106100.
3. ZHANG, Y.Y., LI, J., LV, M.Y., TAN, D.J., ZHU, W.Y. and SUN, K.W. Simplified analytical model for investigating the output power of solar array on stratospheric airship. *Int J Aeronaut Space Sci*, 2016, **17**, (3), pp 432–441.
4. YANG, X.X. and LIU, D.N. Renewable power system simulation and endurance analysis for stratospheric airships. *Renew Energy*, 2017, **113**, (12), pp 1070–1076.
5. ZHENG, Z.W., CHEN, T., XU, M. and ZHU, M. Modeling and path-following control of a vector-driven stratospheric satellite. *Adv Space Res*, **57**, (9), 1901–1913, 2016.
6. YANG, Y.Y. Positioning control for stratospheric satellites subject to dynamics uncertainty and input constraints. *Aerosp Sci Technol*, 2019, **86**, pp 534–541.
7. LIU, Y., WU, Y.L. and HU, Y.M. Autonomous dynamics-modeling and feedback control for an airship. *Control Theory Appl*, 2010, **27**, (8), pp 991–997.
8. FAN, Y.H., YU, Y.F. and YAN, J. High altitude satellite altitude control system design and simulation. *Sci Technol Eng*, 2011, **11**, (24), pp 5957–5961.
9. GUO, J.G. and ZHOU, J. Compound control system of stratospheric satellite based on aircrew systems. *J Astronaut*, 2009, **30**, (1), pp 225–230.

https://doi.org/10.1017/aer.2021.9 Published online by Cambridge University Press

10. DI, X.G., HAN, F. and YAO, Y. Attitude control allocation strategy of high altitude satellite based on synthetic performance optimization. *J Harbin Inst Technol*, 2009, **16**, (6), pp 746–750.
11. CHEN, L., DONG, Q., ZHANG, G. and DUAN, D. Composite control system of hybrid-driven mid-altitude airship. *Aeronaut J*, **122**, (1248), 173–204, 2018.
12. WHITE, J.E. and ROBINETT, R.D. Principal axis misalignment control for deconing of spinning spacecraft. *J Guid Control Dyn*, 1994, **17**, (4), pp 823–830.
13. REGAN, F.J. and KAVETSKY, R.A. Add-on controller for ballistic reentry vehicles: USA patent, 1984, pp 752–766.
14. WOOLSEY, C.A. and LEONARD, N.E. Moving mass control for underwater vehicles. In: Proceedings of the 2002 American Control Conference, IEEE, Anchorage, 2002, pp 2824–2829.
15. MENON, P.K. and SWERIDUK, G.D. Integrated guidance and control of moving-mass actuated kinetic warheads. *J Guid Control Dyn*, 2004, **27**, (1), pp 118–126.
16. DENG, Y.G., GU, W.J., ZHAO, H.C. and YU, J.Y. Research on composite control of mass/thrust vectoring for a kind of saucer-like air vehicle. *Flight Dyn*, **23**, (3), pp 28–31, 2005.
17. VADDI, S.S. Moving mass actuated missile control using convex optimization techniques. AIAA Guidance, Navigation, and Control Conference and Exhibit, Keystone, Colorado, 2006, pp 1–13.
18. GAO, M.W. and SHAN, X.X. By changing position research of satellite's center of gravity to control longitudinal motion. *Chin Q Mech*, 2006, **27**, (4), pp 714–718.
19. CHEN, L., ZHOU, G., YAN, X.J. and DUAN, D.P. Composite control strategy of stratospheric airships with moving masses. *J Aircr*, 2012, **49**, (3), pp 794–800.
20. CHEN, L., ZHOU, H., WEN, Y.B. and DUAN, D.P. Control of the horizontal position of a stratospheric airship during ascent and descent. *Aeronaut J*, 2015, **119**, (1214), pp 523–541.

https://doi.org/10.1017/aer.2021.9 Published online by Cambridge University Press